DALTON
FULL PAPER

# Conformationally locked pentadentate macrocycles containing the 1,10-phenanthroline unit. Synthesis and crystal structure of 5-oxa-2,8-dithia[9](2,9)-1,10-phenanthrolinophane (L) and its coordination properties to $Ni^{II}$, $Pd^{II}$, $Pt^{II}$, $Rh^{III}$ and $Ru^{II}$ †

**Massimiliano Arca,[a] Alexander J. Blake,[b] Jaume Casabò,[c] Francesco Demartin,[d] Francesco A. Devillanova,[a] Alessandra Garau,[a] Francesco Isaia,[a] Vito Lippolis,*[a] Raikko Kivekas,[e] Vicent Muns,[c] Martin Schröder[b] and Gaetano Verani[a]**

[a] *Dipartimento di Chimica Inorganica ed Analitica, Complesso Universitario di Monserrato, Università di Cagliari, S.S. 554 bivio per Sestu, 09042 Monserrato (CA), Italy. E-mail: lippolis@vaxca1.unica.it*
[b] *School of Chemistry, The University of Nottingham, University Park, Nottingham, UK NG7 2RD*
[c] *Departemento de Quimica (Unit Inorganica), Universitat Autonoma de Barcelona, 08193 Bellaterra, Barcelona, Spain*
[d] *Dipartimento di Chimica Strutturale e Stereochimica Inorganica, Università di Milano, Via G. Venezian 21, 20133 Milano, Italy*
[e] *Department of Chemistry, University of Helsinki, PO Box 55, FIN 00014 Helsinki, Finland*

***Received 15th January 2001, Accepted 26th February 2001***
***First published as an Advance Article on the web 26th March 2001***

The complexation of the new mixed thia–aza–oxa macrocycle 5-oxa-2,8-dithia[9](2,9)-1,10-phenanthrolinophane (**L**) containing the 1,10-phenanthroline unit with $Ni^{II}$, $Pd^{II}$, $Pt^{II}$, $Rh^{III}$ and $Ru^{II}$ has been investigated. The results have been compared with those obtained with the structurally related ligand 2,5,8-trithia[9](2,9)-1,10-phenanthrolinophane (**L′**). The most stable conformations of both ligands have been calculated in order to understand their change upon metal complexation and for **L** good agreement has been found with the conformations observed in the crystal structure of $\mathbf{L}\cdot\frac{1}{2}H_2O$. The single-crystal structures of $[Ni(\mathbf{L})Cl]BF_4$ and $[Ru(\mathbf{L})(PPh_3)][PF_6]_2\cdot\frac{1}{4}MeCN$ reveal a $N_2S_2O$ coordination sphere about $Ni^{II}$ and $Ru^{II}$, with the macrocyclic ligand in a folded conformation and with the sixth coordination site taken up by $Cl^-$ or $PPh_3$, respectively. For $[Pd(\mathbf{L})][BF_4]_2$ an $[N_2S_2 + O]$ coordination is observed, with the O-donor interacting weakly with the metal centre at the apical position of a square-based coordination sphere. $^{13}C$ and $^1H$ NMR spectroscopic studies indicate that the complexes are not fluxional in solution, with the ligand imposing the same coordination sphere as observed in the solid state. $^{13}C$ NMR spectroscopy has also helped in elucidating the stereochemistry of $[Rh(\mathbf{L})Cl_2]BF_4$ for which no suitable crystals could be grown: the two $Cl^-$ ligands are mutually *trans* with the $N_2S_2$ donor set of the macrocyclic ligand occupying the equatorial positions of an octahedral coordination sphere and with the O-donor atom left un-coordinated. The redox properties of all the complexes in MeCN have been studied.

## Introduction

The quest for new macrocyclic ligands capable of specific and effective molecular recognition of metal ions in carrier-assisted membranes or solid-state ion-selective electrodes is a topic of current interest.[1,2] Attention has mainly been focussed on assisted transfer of Group I and II ions between two immiscible electrolyte solutions, and different crown ether derivatives have been used as neutral carriers for the construction of ion selective electrodes and for performing selective separations.[1–4] A smaller number of studies have reported on transition and heavy metal ions, particularly precious metal ions probably because of their greater inertness.[5,6] However, the recovery and removal of precious metals from aqueous solutions is of considerable economic and environmental concern. It is well known that the formation constant of complexes of Group I and II ions with crown ethers drastically decreases upon replacement of some of the oxygen atoms of the cyclic ligands with sulfur donors.[7] On the other hand, thioether macrocycles have come to great prominence in the last decade due to their ability to stabilise unusual oxidation states and coordination geometries of soft metal ions such as transition metals and coinage metals.[8,9] Some thioether crowns containing rigid aromatic and heteroaromatic units fused with thioether linkers have also been tested as sensors in solid-state electrodes, resulting in particularly selective detection of $Ag^I$.[10–12] Recently we have reported the synthesis and coordination properties towards $Ni^{II}$, $Pd^{II}$, $Pt^{II}$ and $Rh^{III}$ of new mixed aza-thioether crowns containing the 1,10-phenanthroline (phen) unit as an integral part of the macrocyclic structure.[13–15] In particular, the pentadentate ligand 2,5,8-trithia[9](2,9)-1,10-phenanthrolinophane (**L′**) has been shown to have coordination properties strictly dependent upon the conformational constraints imposed by the heteroaromatic moiety on the S-donor thioether linker of the ring. Furthermore, the presence in the cyclic framework of **L′** of the phen unit, which carries hard N-donor atoms and is an excellent π acceptor, has been shown to confer on this macrocycle the ability to stabilise low-valent

† Electronic supplementary information (ESI) available: elemental analysis data and optimised dihedral angles of conformers of L and L′. See http://www.rsc.org/suppdata/dt/b1/b100493j/

 DOI: 10.1039/b100493j

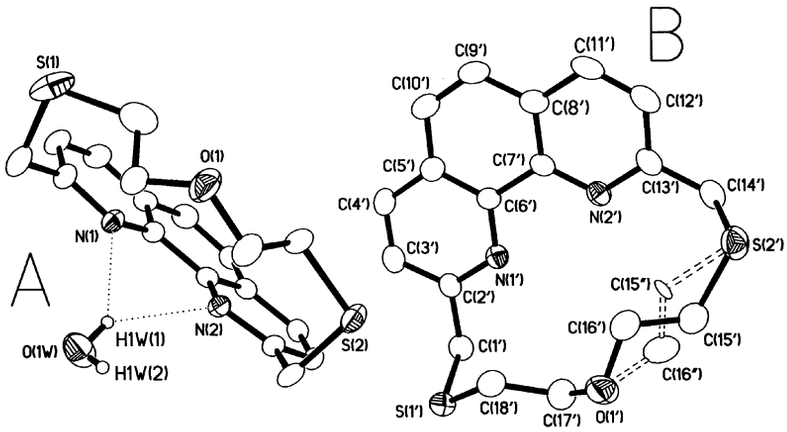


**Fig. 1** View of the two independent macrocyclic molecules (A and B) and water molecule in the crystal structure of $\mathbf{L}\cdot\frac{1}{2}H_2O$. The numbering scheme adopted for A uses the corresponding unprimed labels. Atoms C(15″) and C(16″) in molecule B comprise the minor disorder component. Displacement ellipsoids are drawn at 50% probability and hydrogen atoms in the macrocyclic framework are omitted for clarity.

metal complexes.[14,15] The assisted transfer of $Rh^{III}$ by interfacial complexation with **L′** at the polarised water/1,2-dichloromethane junction is presently under investigation and preliminary results indicate that **L′** can selectively assist the transfer of $Rh^{III}$ across an organic membrane from an aqueous solution.[16] In view of the possible analytical applications of this new class of macrocycles containing the 1,10-phenanthroline unit, we consider it to be of primary importance to study further their coordination properties towards $d^8$ transition metal ions in order to understand better their selectivity properties. These aspects will play important roles in the complex mechanism of molecular recognition. We report herein the synthesis and crystal structure of the new macrocycle 5-oxa-2,8-dithia[9]-(2,9)-1,10-phenanthrolinophane (**L**) which differs from **L′** in that the aliphatic portion of the ring contains a hard O-donor instead of a softer S-donor. The coordination properties of **L** with $Ni^{II}$, $Pd^{II}$, $Pt^{II}$, $Rh^{III}$ and $Ru^{II}$ are described and compared with the properties of **L′**. The most stable conformations of both ligands have been calculated in order to understand both the flexibility of these macrocycles and the conformational changes that occur upon complexation.

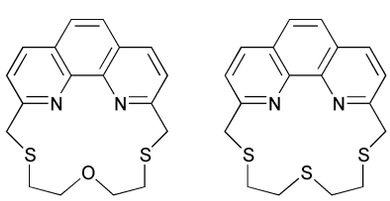


## Results and discussion

### Ligand synthesis and conformations

The strategy adopted in the synthesis of **L** is similar to that reported for **L′** [13] and involves a cyclisation reaction performed under high dilution conditions between 2,9-bis(chloromethyl)-1,10-phenanthroline and $(HSCH_2CH_2)_2O$ in dmf in the presence of $Cs_2CO_3$. The macrocycle obtained was crystallised from MeCN to give crystals suitable for single crystal X-ray diffraction studies. The crystal structure shows the presence of two independent **L** molecules (identified as A and B in Fig. 1) and one molecule of water in the asymmetric unit. One of the two **L** molecules (B) exhibits disorder in the aliphatic portion of the ring between O(1′) and S(2′) whereas the other (A) forms hydrogen bonds with the water molecule through N(1) and N(2); crystal packing also involves extensive hydrogen bonds with the oxygen atom of the macrocyclic molecules. The intramolecular distances and angles of both independent units of **L** are typical for this type of organic compound. However, certain conformational characteristics are worthy of comment. The phenanthroline moieties and carbon atoms C(1) and C(14) in unit A [C(1′) and C(14′) in unit B] lie on a plane. The rest of the aliphatic chain is folded over the phenanthroline unit with angles of 65 and 66° between the phenanthroline ring and the mean planes containing C(1), S(1), S(2), C(14) and C(1′), S(1′), S(2′), C(14′) for the two independent units A and B, respectively. A similar disposition of the aliphatic portion of the macrocycle with respect to the plane of the heteroaromatic moiety has been observed in 6-oxa-3,9-dithia-15-aza-bicyclo-[9.3.1]pentadeca-1(15),11,13-triene[17] which differs from **L** in having a pyridine unit instead of the phenanthroline moiety. The explanation given for the conformational behaviour of the macrocycle containing the pyridine framework (in terms of repulsion between the two sulfur atoms in the ring) cannot apply to **L** in which the S-donors would be too far apart even in a completely planar conformation of the ligand. Presumably, the conformations adopted by **L** in the solid state are mainly determined by two predominant factors: (a) the constraints imposed by the phenanthroline moiety on the flexibility of the aliphatic chain and (b) the tendency of the lone pairs on the S-donors to occupy exodentate positions pointing out of the ring cavity with the effect of maximising the number of *gauche* placements about the C–S bonds as generally observed for thioether macrocycles.[8,18]

In order to understand better the conformational behaviour of these new phenanthroline-based macrocycles, we undertook molecular mechanics (MM) calculations (see Experimental section) on both **L** and **L′**, in the hope of obtaining low-energy "lattice-free" conformers that would be comparable to those observed in the solid state. Fig. 2 shows the four most stable conformers calculated for **L** (**1a**–**1d**) and **L′** (**2a**–**2d**) which differ in energy by less than 2 kcal $mol^{-1}$. Two features are common to all calculated conformations in Fig. 2: (a) for both **L** and **L′** the aliphatic chain of the ring is tilted over the plane containing the phenanthroline unit which forms an angle ranging from 67.75 (**1b**) to 78.74° (**1a**) with the mean plane through the atoms C(1), S(1), C(14) and S(2); (b) in these calculated conformations which have the lowest conformational energies, the lone pairs on both the S- and O-donors tend to adopt exodentate orientations pointing out of the macrocyclic cavity. In particular, from an inspection of the calculated torsion angles which define the eight conformers in Fig. 2 (deposited as Electronic Supplementary Information), one can see that all the torsion angles S(2)–C(15)–C(16)–X and X–C(17)–C(18)–S(1) [X = O (**L**) or S (**L′**), see Fig. 2] assume *anti* arrangements with absolute values of the angle ranging from 159.64 (**2d**) to 179.74° (**2b**). A *gauche* disposition is instead preferred at the C–S(1) and C–S(2) bonds, with the possible exception of the torsion angles around the

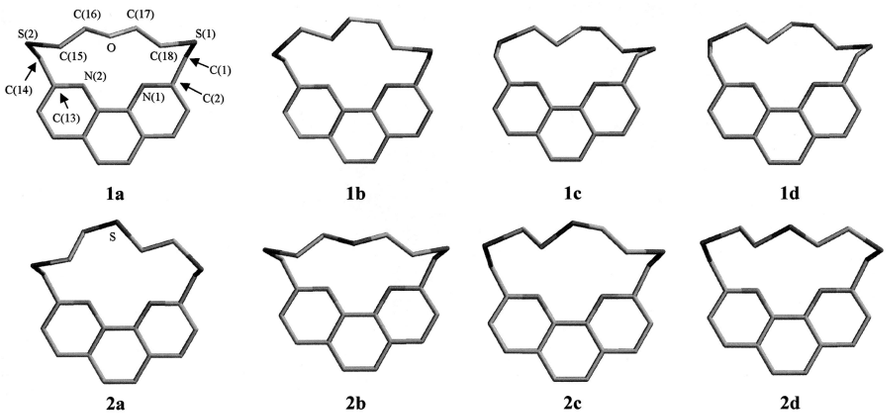


**Fig. 2** View of the most four stable calculated conformers for **L** (**1a**–**1d**) and **L′** (**2a**–**2d**). The numbering scheme for the two ligands is the same as in Fig. 1. Hydrogen atoms are omitted for clarity.

**Table 1** Selected bond lengths (Å) and angles (°) for $[Ni(\mathbf{L})Cl]BF_4$, $[Pd(\mathbf{L})][BF_4]_2$, $[Ru(\mathbf{L})(PPh_3)][PF_6]_2\cdot\frac{1}{4}MeCN$ and $[Ru(\mathbf{L}')Cl]Cl\cdot 4H_2O$

| | $[Ni(\mathbf{L})Cl]BF_4$ | $[Pd(\mathbf{L})][BF_4]_2$ [a] | $[Ru(\mathbf{L})(PPh_3)][PF_6]_2\cdot\frac{1}{4}MeCN$ | $[Ru(\mathbf{L}')Cl]Cl\cdot 4H_2O$ |
|---|---|---|---|---|
| M–N(1) | 2.038(4) | 1.984(4) [1.975(6)] | 2.026(6) | 2.018(5) |
| M–N(2) | 2.019(4) | 1.982(4) | 2.021(6) | 2.017(5) |
| M–S(1) | 2.4371(13) | 2.2951(14) [2.312(2)] | 2.336(2) | 2.355(2) |
| M–S(2) | 2.4633(13) | 2.3077(14) | 2.344(3) | 2.345(2) |
| M–O(1) [b] | 2.159(3) | 2.935(4) [3.01(2)] | 2.172(5) | |
| M–S(3) [c] | | | | 2.299(2) |
| M–X [d] | 2.3342(14) | | 2.264(3) | 2.446(2) |
| S(1)–M–N(1) | 80.74(11) | 82.53(13) [83.3(2)] | 82.2(2) | 82.36(14) |
| S(1)–M–N(2) | 160.23(11) | 163.19(14) [166.4(2)] | 161.6(2) | 163.17(14) |
| S(1)–M–X | 94.69(5) | | 93.78(8) | 91.57(6) |
| S(1)–M–S(2) | 116.72(5) | 111.01(6) [109.96(11)] | 112.66(8) | 113.68(6) |
| S(1)–M–O(1) | 81.77(9) | 73.63(9) [69.1(2)] | 84.0(2) | |
| S(1)–M–S(3) | | | | 86.74(6) |
| S(2)–M–N(1) | 160.33(11) | 165.65(13) | 161.5(2) | 163.95(14) |
| S(2)–M–N(2) | 81.23(11) | 83.80(14) | 82.7(2) | 83.08(14) |
| S(2)–M–X | 89.17(5) | | 92.22(12) | 89.17(6) |
| S(2)–M–O(1) | 81.29(9) | 73.27(9) | 84.1(2) | |
| S(2)–M–S(3) | | | | 87.66(6) |
| O(1)–M–N(1) | 93.13(13) | 116.63(14) [115.2(3)] | 86.8(2) | |
| O(1)–M–N(2) | 93.64(13) | 119.8(2) | 87.8(2) | |
| O(1)–M–X | 166.90(9) | | 174.51(14) | |
| S(3)–M–N(1) | | | | 94.27(14) |
| S(3)–M–N(2) | | | | 92.69(13) |
| S(3)–M–X | | | | 175.46(6) |
| N(1)–M–N(2) | 80.33(15) | 82.2(2) [83.2(4)] | 80.9(2) | 80.9(2) |
| N(1)–M–X | 98.77(11) | | 97.9(2) | 89.68(14) |
| N(2)–M–X | 93.76(11) | | 95.7(2) | 90.15(14) |

[a] Values in square brackets refer to the $[Pd(L)]^{2+}$ cation in the monoclinic crystals; for this structure the atoms N(2) and S(2) have been labelled $N(1^i)$ and $S(1^i)$, respectively in Fig. 4(b) [i $x$, $-y+1$, $z$]. [b] The same numbering scheme has been adopted for all the complexes with **L** (Fig. 1). [c] The numbering scheme adopted for **L′** is the same of **L** except for O(1) which is replaced by S(3). [d] X = Cl (for $[Ni(\mathbf{L})Cl]BF_4$ and $[Ru(\mathbf{L}')Cl]Cl\cdot 4H_2O$) and $PPh_3$ (for $[Ru(\mathbf{L})(PPh_3)][PF_6]_2\cdot\frac{1}{4}MeCN$).

bonds S(1)–C(18) (**1d**), C(1)–S(1) (**2a**), S(2)–C(14) (**1b**), C(15)–S(2) (**1c**, **2c**, **2d**) for which the calculated values are −111.00, −106.31, 102.00, 106.45, −103.48 and −110.66°, respectively. Less clear is the trend for the torsion angles about the C–X bonds [X = O (**L**) or S (**L′**), see Fig. 2]; with the exception of the conformers **1a** and **2b** each of which has a plane of symmetry that passes through the X atom and bisects the phenanthroline moiety, the conformers in Fig. 2 have torsion angles about the C–X bonds of which one is generally *gauche* and one *anti* (in **1a** and **2b** they are both *anti*). Interestingly, the conformation adopted by unit A in the crystal structure of **L** (Fig. 1) is very similar to the most stable calculated conformer **1a** [the observed differences might be due to the presence of a water molecule in the crystal structure of **L** which forms hydrogen bonds with the nitrogen atoms of unit A (Fig. 1)], while that adopted by B, considering the major component of the disorder model, is practically identical to the second most stable calculated conformer **1b** (see Fig. 2). Considering the crystal structure of **L** and the molecular mechanics calculations on both **L** and **L′**, it is clear that in these new ligands the phenanthroline unit strongly affects the conformational flexibility of the aliphatic portion of the ring and conformational pre-organisation is required prior to complexation in order for the lone pairs on the donor atoms in the aliphatic chain to point into the macrocyclic cavity.

## Synthesis and characterisation of complexes

In order to compare the coordination properties of **L** with those reported for **L′**, the complexes $[Ni(\mathbf{L})Cl]BF_4$, $[Pd(\mathbf{L})][BF_4]_2$, $[Pd(\mathbf{L})][BF_4]_2\cdot\frac{1}{2}MeCN$, $[Pt(\mathbf{L})][BF_4]_2$ and $[Rh(\mathbf{L})Cl_2]BF_4$ have been synthesized, and the first three characterised by single crystal structure determinations. The coordination properties of both **L** and **L′** towards $Ru^{II}$ have also been investigated and the complexes $[Ru(\mathbf{L})(PPh_3)][PF_6]_2\cdot\frac{1}{4}MeCN$ and $[Ru(\mathbf{L}')Cl]Cl\cdot 4H_2O$ have been synthesized and structurally characterised.

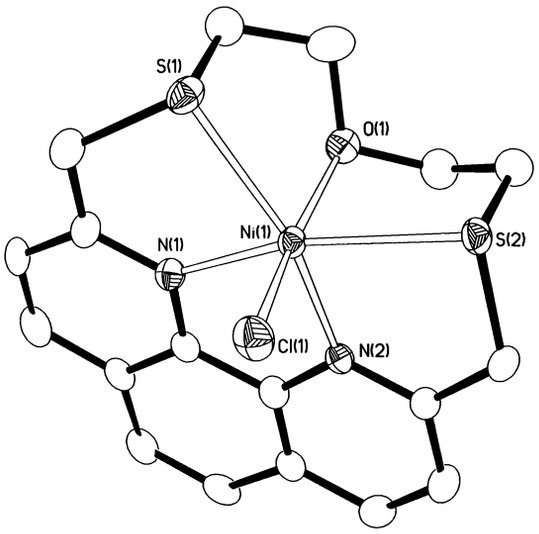


**Fig. 3** View of the $[Ni(\mathbf{L})Cl]^+$ complex cation with the numbering scheme adopted. Displacement ellipsoids are drawn at 50% probability and hydrogen atoms are omitted for clarity.

Figs. 3–5 show the coordination spheres around $Ni^{II}$, $Pd^{II}$ and $Ru^{II}$ in the complexes $[Ni(\mathbf{L})Cl]BF_4$, $[Pd(\mathbf{L})][BF_4]_2$ and $[Ru(\mathbf{L})(PPh_3)][PF_6]_2\cdot\frac{1}{4}MeCN$, respectively, and Table 1 summarises selected bond lengths and angles for all structurally characterised complexes. In $[Ni(\mathbf{L})Cl]^+$ the macrocyclic ligand acts as an $N_2S_2O$ donor, encapsulating the metal ion within a cavity having a square-based pyramidal stereochemistry with the sixth position of the overall distorted octahedral coordination sphere taken up by a $Cl^-$ donor which occupies a *trans* position with respect to the oxygen atom of the ligand (Fig. 3). A similar distorted octahedral geometry at $Ni^{II}$ has been observed for the complex $[Ni(\mathbf{L}')(MeCN)]^{2+}$ obtained by treating $\mathbf{L}'$ with $NiCl_2$ in MeCN, and for all the other related pseudo-octahedral complexes of the type $[Ni(\mathbf{L}')X]^{(2-n)+}$ ($X = H_2O$, pyridine, aniline, 1,3-dimethyl-4-imidazoline-2-thione, 1,3-dimethyl-4-imidazoline-2-selone, $Cl^-$, $Br^-$, $I^-$, $CN^-$ or $SCN^-$) obtained by substituting the acetonitrile molecule with different neutral ($n = 0$) or mono-anionic ($n = 1$) donors.[13,15] However, a slightly shorter Ni–Cl distance [2.3342(14) Å] is observed in $[Ni(\mathbf{L})Cl]^+$ compared to the value of 2.3693(10)Å in $[Ni(\mathbf{L}')Cl]^+$[15] which may reflect the harder character of the O-donor atom *trans* to the $Cl^-$ ligand in $[Ni(\mathbf{L})Cl]^+$ compared to sulfur in the same coordination position in $[Ni(\mathbf{L}')Cl]^+$. Although no significant differences are observed in the conformation adopted by **L** and $\mathbf{L}'$ upon complexation to $Ni^{II}$, the presence of an O-donor instead of an S-donor *trans* to the coordination site left free by the macrocycle ligands drives the complexation reaction of **L** with $NiCl_2$ in MeCN towards the formation of $[Ni(\mathbf{L})Cl]^+$ instead of $[Ni(\mathbf{L})(MeCN)]^{2+}$.[13] Contrary to what is observed for the acetonitrile molecule in the $[Ni(\mathbf{L}')(MeCN)]^{2+}$ cation,[15] the chloride donor in $[Ni(\mathbf{L})Cl]^+$ cannot easily be substituted by direct reaction with other neutral or charged donors, preventing the use of the $[Ni(\mathbf{L})]^{2+}$ cation for binding and activation of small molecules at the coordinatively unsaturated metal centre or as a building block for more complex systems. Interestingly, despite the restricted conformational flexibility of **L**, the apical Ni–O bond distance observed in $[Ni(\mathbf{L})Cl]^+$ [2.159(3) Å] is also significantly shorter than that observed in the complex cations $[Ni([15]aneN_2OS_2)(NO_3)]^+$ [2.24 Å][19] and $[Ni(ether)I]^+$ [2.387(5) Å][20] ([15]aneN$_2$OS$_2$ = 1-oxa-4,13-dithia-7,10-diazacyclopentadecane; ether = 7-oxa-4,10-dithia-1,13-diazabicyclo[11.3.3]nonadecane), in which the more flexible macrocyclic ligands impose a similar square-pyramidal $N_2S_2O$ environment at the metal centre with the sixth position of the octahedron occupied by $NO_3^-$ and $I^-$, respectively.

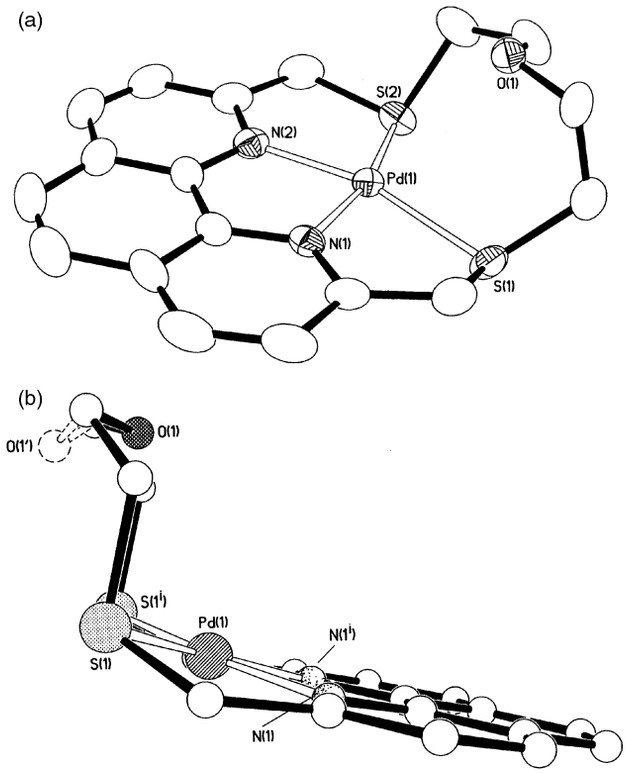


**Fig. 4** (a) View of the $[Pd(\mathbf{L})]^{2+}$ cation (triclinic crystals) with the numbering scheme adopted. Displacement ellipsoids are drawn at 30% probability and hydrogen atoms are omitted for clarity. (b) View of the $[Pd(\mathbf{L})]^{2+}$ cation (monoclinic crystals) showing the two components of the disordered oxygen atom; heavy atoms are not shown as ellipsoids and hydrogen atoms are omitted for clarity [i $x, -y + 1, z$].

The reported single-crystal structures of $[M(\mathbf{L}')][PF_6]_2$ (M = Pd or Pt) show an $[N_2S_2 + S]$ coordination in both complexes, with $\mathbf{L}'$ adopting a folded conformation to allow a long-range M···S apical interaction.[14] In order to study the effect of exchanging the apical sulfur atom for oxygen in these complexes, we have treated **L** with $PdCl_2$ or $PtCl_2$ in refluxing MeCN–water. Complexes corresponding to the formulation $[M(\mathbf{L})][BF_4]_2$ (M = Pd or Pt) have been obtained after addition of an excess of $NH_4BF_4$, partial removal of the solvent and re-crystallisation of the resulting products from MeCN–$Et_2O$. However, only in the case of palladium(II) was it possible to grow crystals suitable for X-ray diffraction studies. Interestingly, the crystals obtained have two slightly different morphologies corresponding to triclinic (block-like) and monoclinic (laminar) systems. The structure of the triclinic crystals confirms the formation of the $[Pd(\mathbf{L})]^{2+}$ cation (Fig. 4a, Table 1). The two N-donors of the phen unit and the two S-donors of the aliphatic linker are bound to the metal ion in a square-planar arrangement with Pd–N [1.984(4), 1.982(4) Å] and Pd–S [2.2951(14), 2.3077(14) Å] bond distances very close to those observed in the $[Pd(\mathbf{L}')]^{2+}$ cation.[14] The remaining O-donor from the macrocyclic ring is oriented towards the metal and lies above the $N_2PdS_2$ coordination plane at a Pd···O distance of 2.935(4) Å which is less than the sum [3.10 Å] of the relevant van der Waals radii.[21] A similar type of apical Pd···O interaction has been observed in the half-sandwich complex $[Pd([9]aneS_2O)Cl_2]$, in which the macrocyclic ligand assumes a facial [2S + O] coordination mode at the metal centre with the oxygen atom lying above the $Cl_2PdS_2$ coordination plane at a Pd···O distance of 2.968(3) Å.[22] A much shorter Pd···O axial interaction [2.779(4) Å] is observed in $[Pd([15]aneN_2OS_2)]^{2+}$.[23] Compared to the Pd···S apical distance in $[Pd(\mathbf{L}')]^{2+}$ [2.865(1) Å][14] the Pd···O separation in $[Pd(\mathbf{L})]^{2+}$ is significantly longer, consistent with the greater preference of $Pd^{II}$ for soft donors. Furthermore, the Pd(1)–O(1) vector in

**Table 2** $^{13}C$ NMR chemical shifts for **L** and **L′** and their complexes with $Pd^{II}$, $Pt^{II}$, $Rh^{III}$ and $Ru^{II}$ in $CD_3CN$ solution at 298 K

| Compound | C(16)/C(17) | C(15)/C(18) | C(1)/C(14) | C(2)/C(13) | C(3)/C(12) | C(4)/C(11) | C(5)/C(8) | C(9)/C(10) | C(6)/C(7) |
|---|---|---|---|---|---|---|---|---|---|
| **L** | 70.7 | 29.3 | 36.9 | 158.9 | 122.8 | 137.4 | 127.4 | 126.0 | 144.6 |
| $[Pd(\mathbf{L})]^{2+}$ [a] | 65.4 | 40.6 | 50.5 | 164.9 | 125.5 | 141.6 | 131.2 | 128.7 | 147.5 |
| $[Pt(\mathbf{L})]^{2+}$ [a] | 66.4 | 41.9 | 52.1 | 163.9 | 124.9 | 141.7 | 131.2 | 128.7 | [b] |
| $[Rh(\mathbf{L})Cl_2]^{+}$ [a] | 65.8 | 36.2 | 50.1 | 161.5 | 125.7 | 139.9 | 131.0 | 128.4 | 146.4 |
| $[Ru(\mathbf{L})(PPh_3)]^{2+}$ [a] | 76.6 | 40.4 | 49.9 | 163.6 | 123.9 | 137.3 | 130.7 | 128.5 | 147.6 |
| **L′** [c] | 32.0 | 33.7 | 37.1 | 159.5 | 122.6 | 137.1 | 127.3 | 125.8 | 144.6 |
| $[Pd(\mathbf{L}')]^{2+}$ [c] | 27.7 | 40.8 | 49.5 | 164.3 | 125.3 | 141.1 | 131.2 | 128.6 | 147.3 |
| $[Pt(\mathbf{L}')]^{2+}$ [c] | 27.3 | 41.6 | 50.8 | 164.1 | 124.8 | 141.3 | 131.3 | 128.7 | 146.3 |
| $[Rh(\mathbf{L}')Cl]^{2+}$ [c] | 39.6 | 40.7 | 51.6 | 161.5 | 126.3 | 141.0 | 132.0 | 128.8 | 146.4 |
| $[Ru(\mathbf{L}')Cl]^{+}$ [a] | 37.1 | 35.7 | 49.6 | 160.9 | 122.3 | 133.5 | 128.8 | 126.6 | 146.5 |

[a] This work. [b] The signal corresponding to C(6)/C(7) in $[Pt(\mathbf{L})]^{2+}$ could not be observed. [c] Ref. 14.

$[Pd(\mathbf{L})]^{2+}$ shows a deviation of 34.3° from perpendicularity with respect to the palladium(II) coordination plane [a deviation of only 14.3° is observed for the Pd(1)–S(3) vector in $[Pd(\mathbf{L}')]^{2+}$], while the basal angles S(1)–Pd(1)–N(2) [163.19 (14)°] and S(2)–Pd(1)–N(1) [165.65(13)°] are very close to the value of 164° given by Rossi and Hoffmann[24] as the optimum for a square-based pyramidal geometry around a $d^8$ ion. The coordination geometry of the $Pd^{II}$ and the disposition of the macrocyclic ligand **L** (the lone pair on O(1) is clearly oriented towards the $d_{z^2}$ orbital of the palladium) indicate that some form of apical interaction between the metal centre and the O(1) donor atom is present in $[Pd(\mathbf{L})]^{2+}$; however, this interaction is very weak, as indicated by NMR studies (*vide infra*). The monoclinic crystals of $[Pd(\mathbf{L})][BF_4]_2$ differ from the triclinic ones in that the unit cell contains two molecules of MeCN and the $[Pd(\mathbf{L})]^{2+}$ cation sits across a plane of reflection passing through the metal and the O(1) atoms and bisecting the N–Pd–N angle (see Fig. 4b). The Pd(1)···O(1) interaction in the monoclinic crystals [3.01(2) Å] is significantly longer than that in the triclinic ones, the Pd(1)–O(1) vector deviating by 36.2° from perpendicularity with respect to the palladium coordination plane. Furthermore, the O(1) donor atom in the monoclinic crystals is disordered over two sites, with the minor component of the disorder model O(1′) (see Fig. 4b) oriented away from the axial site of the $N_2PdS_2$ coordination plane. These structural features of the $[Pd(\mathbf{L})]^{2+}$ cation clearly demonstrate the inability of the $CH_2CH_2OCH_2CH_2$ fragment of the aliphatic portion of **L** to orient itself as to encapsulate fully the axial site of a square pyamidal coordination geometry around $Pd^{II}$: this could be attributed to the weakness of the interaction between the oxygen atom and the metal centre.

We reported previously[14] the reaction of **L′** with $RhCl_3$ in refluxing MeCN–water to afford a yellow microcrystalline powder after addition of an excess of $NH_4PF_6$. The formulation $[Rh(\mathbf{L}')Cl][PF_6]_2$ for the resulting complex was based on elemental analysis data and on IR and FAB mass spectroscopy. $^{13}C$ NMR spectroscopic measurements in $CD_3CN$ confirmed this formulation and indicated an octahedral stereochemistry at the $Rh^{III}$ similar to that observed around $Ni^{II}$ in $[Ni(\mathbf{L})Cl]^{+}$,[15] with all S-donors of the macrocyclic ligand strongly coordinated and with a chloride completing the octahedral environment. The same reaction has been repeated using **L**, yielding yellow platy crystals unsuitable for X-ray diffraction studies. The fast-atom bombardment (FAB) mass spectrum of the complex exhibits peaks with the correct isotopic distribution for $[Rh(\mathbf{L})Cl_2]^{+}$ (*m*/*z* 515) and $[Rh(\mathbf{L})Cl]^{+}$ (*m*/*z* 480), suggesting the formulation $[Rh(\mathbf{L})Cl_2]BF_4$. As confirmed by NMR measurements (*vide infra*), it appears that the O-donor in **L** is not able to coordinate the metal centre by replacing one chloride from the starting $RhCl_3$ salt, thus remaining un-coordinated in the $[Rh(\mathbf{L})Cl_2]^{+}$ complex cation. Interestingly, this different coordination behaviour of **L′** and **L** is not observed for $Ru^{II}$: the reaction of $RuCl_2(PPh_3)_4$ with **L′** in refluxing MeOH affords, after slow evaporation of the solvent, red crystals of $[Ru(\mathbf{L}')Cl]Cl{\cdot}4H_2O$ according to analytical and spectroscopic data. In contrast, the reaction of $RuCl_2(PPh_3)_4$ with **L** in refluxing MeOH gives, after addition of excess of $NH_4PF_6$, a yellow microcrystalline compound corresponding to the formulation $[Ru(\mathbf{L})(PPh_3)][PF_6]_2$: this complex can be re-crystallised by slow diffusion of $Et_2O$ vapour into a MeCN/MeOH solution. X-Ray diffraction studies were undertaken to ascertain the ligation and stereochemistry of both complexes and confirm the formation of the cations $[Ru(\mathbf{L}')Cl]^{+}$ and $[Ru(\mathbf{L})(PPh_3)]^{2+}$ (see Table 1 and Fig. 5 for the latter), with the ligands **L′** and **L** acting as $N_2S_3$- and $N_2S_2O$-donors, respectively, and encapsulating the metal centre within a cavity which confers a square-based pyramidal stereochemistry. An octahedral coordination sphere around $Ru^{II}$ is completed by a $Cl^{-}$ ion *trans* to an S-donor in $[Ru(\mathbf{L}')Cl]^{+}$ and by a triphenylphosphine ligand *trans* to the O-donor in $[Ru(\mathbf{L})(PPh_3)]^{2+}$. While the octahedral coordination around $Ru^{II}$ and $Rh^{III}$ in $[Ru(\mathbf{L}')Cl]^{+}$, $[Ru(\mathbf{L})(PPh_3)]^{2+}$ and $[Rh(\mathbf{L}')Cl]^{2+}$ [14] is very similar to that observed around $Ru^{II}$ in the complex cation $[Ru([15]aneS_5)(PPh_3)]^{2+}$,[25] in $[Rh(\mathbf{L})Cl_2]^{+}$ two isomers are possible, with the two $Cl^{-}$ ions being either mutually *cis* or *trans* and the O-donor of the macrocyclic ligand away from the coordination sphere. Both types of isomers have been observed for the rhodium(III) complexes $[Rh([14]aneS_4)Cl_2]^{+}$ [26] and $[Rh(cyclam)Cl_2]^{+}$,[27] but only the *trans*-dichloro geometry for $[Rh([16]aneS_4)Cl_2]^{+}$,[26] $[Rh([16]aneSe_4)Cl_2]^{+}$ [28] and $[Rh(pyN_4)Cl_2]^{+}$ [29] ($pyN_4$ = 2,3,7,11,12-pentamethyl-1,3,7,11-tetraazabicyclo[11.3.1]heptadeca-1(17),13,15-triene) where the tetradentate macrocyclic ligands occupy the equatorial plane.

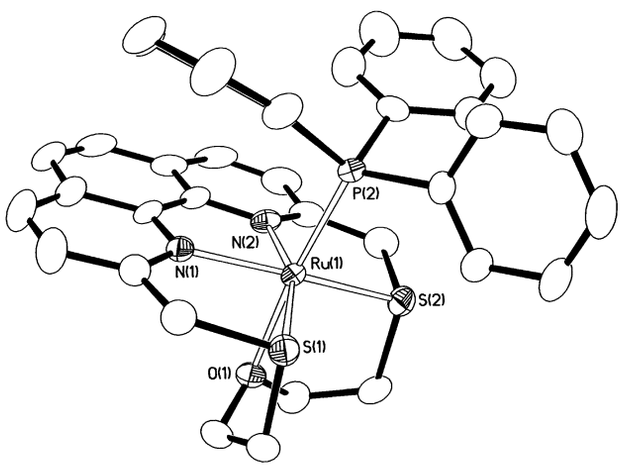


**Fig. 5** View of the $[Ru(\mathbf{L})(PPh_3)]^{2+}$ cation with the numbering scheme adopted. Displacement parameters are drawn at 50% probability and hydrogen atoms are omitted for clarity.

### $^{13}C$ and $^{1}H$ NMR measurements

The $^{13}C$ NMR chemical shifts for **L** and **L′** and their complexes with $Pd^{II}$, $Pt^{II}$, $Rh^{III}$ and $Ru^{II}$ in $CD_3CN$ solution at 298 K are reported in Table 2 (the crystal structure numbering scheme

has been adopted for their assignment). The spectra of the complexes show no changes in any of their peaks over the temperature range 320–238 K, demonstrating the general absence of fluxionality in solution, but also excluding the possibility that the S(3) atom in **L′** or the O atom in **L** is flipping between being bound and unbound to the metal centres. Furthermore, solid-state $^{13}C$ NMR spectra exhibit the same pattern as those in solution for all the complexes, with good agreement between the chemical shifts. Only six peaks for the aromatic region and three for the aliphatic portion of the macrocyclic ligands are observed in the spectra, indicating that the complexes exist in only one form in solution: this possesses $C_s$ symmetry with a plane of reflection passing through the metal and the S(3)/O atoms and bisecting the N(1)–M–N(2) angle. These spectral features imply a *trans* disposition of the chloride ligands in $[Rh(\mathbf{L})Cl_2]^+$, with the equatorial positions of the octahedral coordination sphere occupied by the $N_2S_2$ donor set of the macrocyclic ligand and the O-donor atom left un-coordinated. With respect to the free macrocycles, the carbon atoms next to S(1) and S(2) [C(15) and C(18)] are deshielded whereas those next to S(3) in the case of **L′** and next to O in the case of **L** [C(16) and C(17)] are shielded for the complexes of $Pd^{II}$ and $Pt^{II}$ and for $[Rh(\mathbf{L})Cl_2]^+$ (Table 2). The situation is different for $[Rh(\mathbf{L}')Cl]^{2+}$ and for the ruthenium(II) complexes in which all above mentioned carbon atoms are deshielded. These data are consistent with the X-ray diffraction studies and in particular with either the O-donor being un-coordinated in $[Rh(\mathbf{L})Cl_2]^+$ or with a [4+1] coordination sphere being imposed by the ligands at the $Pd^{II}$ and $Pt^{II}$ in the solid state as well in solution, with the S(3) (**L′**) and O (**L**) donor atoms weakly interacting with the metal centres.

The $^1H$ NMR spectra of $[Pd(\mathbf{L})]^{2+}$, $[Pt(\mathbf{L})]^{2+}$ and $[Rh(\mathbf{L})Cl_2]^+$, all characterised by the O-donor interacting weakly if at all with the metal centre, exhibit at room temperature three distinct groups of aliphatic protons for the fragment $SCH_2CH_2OCH_2$-$CH_2S$; one of these integrates for four protons. The same feature was observed in the $^1H$ NMR spectra of $[Pd(\mathbf{L}')]^{2+}$ and $[Pt(\mathbf{L}')]^{2+}$ for which the assignment of the chemical shifts was made on the basis of two-dimensional correlation (COSY-45) and $^1H$–$^{13}C$ heteronuclear correlation (HETCOR) experiments:[14] the multiplet integrating for four protons was assigned to the H atoms on the carbons next to the S-donor weakly interacting with the metal centre at the apical position of the square-based pyramidal coordination sphere. In the case of $[Ru(\mathbf{L}')Cl]^+$ four distinct multiplets are observed in the $^1H$ NMR spectrum at room temperature for the $SCH_2CH_2SCH_2$-$CH_2S$ fragment, with each integrating as two protons. Interestingly, this feature is not observed in the $^1H$ NMR spectra of $[Ru(\mathbf{L})(PPh_3)]^{2+}$, where only one very broad multiplet was recorded, or $[Rh(\mathbf{L}')Cl]^{2+}$, where two multiplets integrate for two and six protons respectively:[14] these complexes share with $[Ru(\mathbf{L}')Cl]^+$ the structural feature that all the donor atoms in the aliphatic portion of the ligand interact strongly with the metal centre. For all the complexes studied, the absence of any observed coalescence in the range 320–238 K for any of the peaks is further evidence that such complexes are not fluxional in solution. Another feature common to the $^1H$ NMR spectra of all complexes of **L** and **L′** with $Pd^{II}$, $Pt^{II}$, $Rh^{III}$ and $Ru^{II}$ is an AB sub-spectrum for each pair of protons on C(1) and C(14), suggesting that they assume inequivalent dispositions (above and below the plane of the phenanthroline moiety) as a consequence of complexation. The same pattern has been observed in the $^1H$ NMR spectrum of $[Pd\{(py)_2[9]aneN_2S\}]^{2+}$ ($(py)_2[9]aneN_2S$ = 1-thia-4,7-bis(2-pyridylmethyl)diazacyclononane) for the protons of the methylene group in the pendant arms of the ligand.[30] This latter complex also exhibits no fluxional processes observable by NMR techniques and the S-donor of the macrocyclic framework is weakly bound to the metal centre in solution as well as in the solid state.

## Electrochemistry

Cyclic voltammetry of $[M(\mathbf{L})]^{2+}$ ($M = Pd^{II}$ or $Pt^{II}$) in MeCN (0.1 mol $dm^{-3}$ $Bu^n_4NBF_4$) at platinum electrodes shows two irreversible reductions in the available cathodic potential window at $E_{pc} = -0.83$ and $-1.70$ V for $M = Pd^{II}$, $E_{pc} = -1.32$ and $-1.78$ V for $M = Pt^{II}$ *vs.* $Fc^+$–Fc. The first irreversible reduction for $[Pd(\mathbf{L})]^{2+}$ becomes quasi-reversible if the scan direction of the cyclic voltammogram is changed from cathodic to anodic before the onset of the second reduction process. A similar observation was made for the cyclic voltammetry of $[Pd(\mathbf{L}')]^{2+}$.[14] Coulometric measurements in MeCN upon the first reduction indicate that this is a one-electron process for both $[M(\mathbf{L})]^{2+}$ ($M = Pd^{II}$ or $Pt^{II}$) complexes and it can tentatively be assigned to the couples $Pd^{II/I}$ and $Pt^{II/I}$, respectively. Reversible reductions at $E_{1/2} = -0.74$ and $-0.83$ V *vs.* $Fc^+$–Fc have been observed for the complexes $[Pd(Me_2([18]aneN_2S_4)]^{2+}$[31] and $[Pd([9]aneS_3)(phen)]^{2+}$[32] respectively, and assigned to their $Pd^{II/I}$ couples. Unfortunately, all attempts to establish the precise nature of the palladium(I) reduction products for $[Pd(\mathbf{L})]^{2+}$ have been unsuccessful, probably because of their propensity for dimerisation through the formation of a metal–metal bond.[14] Cyclic voltammetry in MeCN of the rhodium(III) complexes with **L′** and **L** shows three irreversible one-electron reduction processes at $E_{pc} = -0.94$, $-1.26$, $-1.76$ V for $[Rh(\mathbf{L}')Cl]^{2+}$ and at $E_{pc} = -0.94$, $-1.28$ and $-1.67$ V *vs.* $Fc^+$–Fc for $[Rh(\mathbf{L})Cl_2]^+$. The first reduction process in both complexes occurs in the range typical of $Rh^{III/II}$ couples (irreversible reductions at $E_{pc} = -1.10$, $-1.18$ and $-0.73$ V *vs.* $Fc^+$–Fc in MeCN have been observed for $[Rh([12]aneS_4)Cl_2]^+$, $[Rh([14]aneS_4)Cl_2]^+$ and $[Rh([15]aneS_5)Cl]^{2+}$, respectively)[8] and can be assigned as a metal-based reduction. By analogy with the complex $[Rh([9]aneS_3)_2]^{3+}$, which shows two reversible, one-electron reductions at $E_{1/2} = -0.71$ and $-1.08$ V *vs.* $Fc^+$–Fc, and assigned to $Rh^{III/II}$ and $Rh^{II/I}$ couples, respectively,[8] the reduction processes at $-1.26$ V for $[Rh(\mathbf{L}')Cl]^{2+}$ and $-1.28$ V for $[Rh(\mathbf{L})Cl_2]^+$ could be considered metal-based and involving the couple $Rh^{II/I}$. The EPR spectra recorded as frozen (77 K) glasses on MeCN solutions obtained after reductive controlled-potential electrolysis on the first reduction peak for both $[Rh(\mathbf{L}')Cl]^{2+}$ and $[Rh(\mathbf{L})Cl_2]^+$ are of insufficient quality to derive reliable parameters; however, the observed broad signals at low fields might support the presence of rhodium(II) species. Cyclic voltammetry in MeCN of $[Ru(\mathbf{L}')Cl]^+$ shows one irreversible oxidation at $E_{pa} = +0.70$ V and one irreversible reduction at $E_{pc} = -1.73$ V *vs.* $Fc^+$–Fc which have been shown to be both one-electron processes by controlled potential electrolysis. The oxidation process occurs in the range typical of $Ru^{III/II}$ couples[33,34] and can tentatively be assigned as metal-based oxidation. The nature of the reduction process is in contrast less clear. Ruthenium(II) complexes with bipy- or phen-based ligands such as $[Ru(Me_2\text{-phen})_3]^{2+}$ and $[Ru(Me_2\text{-bipy})_3]^{2+}$ ($Me_2$-phen = 5,6-dimethyl-1,10-phenanthroline, $Me_2$-bipy = 4,4′-dimethyl-2,2′-bipyridine) are characterised by three reversible one-electron reductions which have been shown to correspond to successive reduction of the three coordinated ligand molecules: these three reductions take place in the potential ranges: $-1.25$ to $-1.373$, $-1.43$ to $-1.552$ and $-1.68$ to $-2.05$ V *vs.* SCE, respectively).[33] Therefore, the reduction wave at $E_{pc} = -1.73$ V observed for $[Ru(\mathbf{L}')Cl]^+$ might be ligand-centred. This hypothesis would also account for the irreversible reduction processes at $E_{pc} = -1.76$ and $-1.67$ V observed for $[Rh(\mathbf{L}')Cl]^{2+}$ and $[Rh(\mathbf{L})Cl_2]^+$, respectively. Unfortunately, it has not been possible to characterise by EPR the reduction products generated by electrolysis at controlled potential, probably because of their low stability. Interestingly, the complex $[Ru(\mathbf{L})(PPh_3)]^{2+}$ also shows an irreversible one-electron reduction in MeCN at $E_{pc} = -1.60$ V *vs.* $Fc^+$–Fc, However, for this complex no oxidation processes are observed in the available anodic potential window. This could be due

to the effect of the $PPh_3$ ligand stabilising the ruthenium(II) centre.

## Conclusion

These results confirm that the new pentadentate mixed donor macrocycles **L** and **L′** coordinate readily to a range of platinum group metal ions to give 1 : 1 complexes. Both ligands tend to impose a square-based pyramidal coordination sphere at the considered metal centres as a consequence of the reduced conformational flexibility caused by the presence of the phenanthroline moiety. Substitution of the soft S-donor in **L′** with the hard O-donor in **L** allows one to alter, and in principle to control, the coordination environment around heavy d transition metals. In particular, for metal ions preferring an octahedral coordination geometry, the coordination at the sixth position left free by the macrocyclic framework can be controlled by substituting **L** with **L′**, thus assisting the host–guest complexation process.

## Experimental

All melting points are uncorrected. Microanalytical data were obtained by using a Fisons EA CHNS-O instrument operating at 1000 °C. Mass spectra were acquired at the EPSRC National Service for Mass Spectrometry at Swansea (UK). $^1$H and $^{13}$C NMR spectra were recorded on a Varian VXR300 spectrometer, $^{13}$C CP-MAS spectra on a Varian Unity Inova 400 instrument operating at 100.5 MHz with samples packed into a zirconium oxide rotor. Uv-visible measurements were carried out at 25 °C using a Varian Model Cary 5 UV-Vis-NIR spectrophotometer. Cyclic voltammetry was performed using a conventional three-electrode cell, with a platinum double-bead electrode and Ag–AgCl reference electrode: all measurements were taken under an argon atmosphere in a 0.1 mol dm$^{-3}$ solution of $Bu^n_4NBF_4$ in dmf or MeCN, which were freshly distilled prior to use from $CaSO_4$ or $CaH_2$, respectively. All potentials were referenced internally using the $Fc^+$–Fc couple. Scan rates ranged from 50 to 400 mV s$^{-1}$. Data were recorded on a computer controlled Model 273 EG & G (Princeton Applied Research) potentiostat-galvanostat using Model 270 electrochemical analysis software. Molecular Mechanics calculations were performed on a Digital 500au Personal Workstation running Digital Unix using the Spartan 5.0 Program.[35] The potential energy surface was sampled by means of a Monte Carlo technique, keeping the phenanthroline unit of **L** and **L′** fixed and exploring the torsional energy surfaces of the remaining aliphatic portion of the macrocyclic compounds. The geometry of each of the 441 most stable conformers obtained has been optimised at the MMFF94 level.[36] 2,9-Dimethyl-1,10-phenanthroline and $(HSCH_2CH_2)_2O$ were obtained from Aldrich. The following compounds were prepared according to the reported procedures: 2,9-diformyl-1,10-phenanthroline,[37] 2,9-bis(hydroxymethyl)-1,10-phenanthroline,[37] 2,9-bis(chloromethyl)-1,10-phenanthroline[38] and $RuCl_2(PPh_3)_4$.[39] All the CHN analysis data have been deposited as Electronic Supplementary Information (ESI) and they are consistent with the formulation given for the complexes.

### Preparations

**5-Oxa-2,8-dithia[9](2,9)-1,10-phenanthrolinophane (L).** To a well stirred suspension of $Cs_2CO_3$ (1.18 g, 3.61 mmol) in dmf (80 cm$^3$) maintained at 55 °C was added under $N_2$ over 15 h a solution of 2,9-bis(chloromethyl)-1,10-phenanthroline (0.5 g, 1.80 mmol) and $(HSCH_2CH_2)_2O$ (0.25 g, 1.80 mmol) in dmf (40 cm$^3$). The resultant mixture was stirred for 1 h at 55 °C and then for 24 h at room temperature and subsequently concentrated under vacuum. The residue was extracted into $CH_2Cl_2$ (100 cm$^3$) and the organic extract washed with water, dried over $MgSO_4$ and concentrated under vacuum. The resulting deep yellow residue was purified by flash chromatography on silica gel using $CH_2Cl_2$–$MeCO_2Et$–EtOH (5 : 1 : 0.25 v/v/v) as eluent to give 0.27 g (43.7% yield) of the desired compound as a pale white product which was shown to be a single component by TLC analysis: mp 185 °C [Found (Calc. for $C_{18}H_{19}N_2O_{1.5}S_2$): C, 62.1 (61.5); H, 5.7 (5.5); N, 8.2 (8.0); S, 18.0 (18.2%)]. $^1$H NMR ($CDCl_3$, 298 K): $\delta_H$ 8.26 (2H, d, $J$ = 8.8, H(3)/H(12)), 7.80 (2H, s, H(9)/H(10)), 7.63 (2H, d, $J$ = 8.0 Hz, H(4)/H(11)), 4.13 (4H, s, H(1)/H(14)), 4.07 (4H, m, H(16)/H(17)), 2.60 (4H, m, H(15)/H(18)). $^{13}$C NMR ($CDCl_3$, 298 K): $\delta_C$ 158.92, 144.61, 137.36, 127.35, 125.96, 122.83, 70.66, 29.25, 36.87. Mass spectrum (electronic impact, EI$^+$): $m/z$ = 342 [M$^+$], 266 [M − $(CH_2)_2O(CH_2)$]$^+$ and 178 [phen]$^+$. Electronic spectrum ($CH_2Cl_2$): $\lambda$ = 235 ($\varepsilon$ = 44800), 272 (21300), 288 (19100), 306 nm (10060 dm$^3$ mol$^{-1}$ cm$^{-1}$).

**[Ni(L)Cl]$BF_4$.** A mixture of **L** (40 mg, 0.117 mmol) and $NiCl_2 \cdot 6H_2O$ (28 mg, 0.117 mmol) in MeCN–water (30 cm$^3$, 1 : 1 v/v) was refluxed under $N_2$ for 2 h. Addition of a large excess of $NH_4BF_4$ to the resulting blue solution and concentration under reduced pressure afforded a blue microcrystalline solid. Recrystallisation by slow diffusion of $Et_2O$ vapour into an $MeNO_2$ solution of the product gave [Ni(**L**)Cl]$BF_4$ (41 mg, 67.7% yield) as well shaped blue blocky crystals. FAB mass spectrum (3-nitrobenyl alcohol, 3-NOBA, matrix): $m/z$ 401; calc. for [$^{58}$Ni(**L**)]$^+$ 401. Electronic spectrum ($MeNO_2$): $\lambda$ = 608 ($\varepsilon$ = 39), 859 (40), 914 nm (shoulder) (38 dm$^3$ mol$^{-1}$ cm$^{-1}$).

**[Pd(L)][$BF_4$]$_2$.** A mixture of **L** (50 mg, 0.146 mmol) and $PdCl_2$ (26 mg, 0.146 mmol) in MeCN–water (40 cm$^3$, 1 : 1 v/v ratio) was refluxed under $N_2$ for 2 h. Addition of a large excess of $NH_4BF_4$ to the resulting solution and partial removal of the solvent under reduced pressure afforded a yellow solid. Recrystallisation by slow diffusion of $Et_2O$ vapour into an MeCN solution of the yellow powder gave [Pd(**L**)][$BF_4$]$_2$ (45 mg, 46.7% yield) as yellow blocky crystals. FAB mass spectrum (3-NOBA matrix): $m/z$ 452; calc. for [$^{106}$Pd(**L**)]$^+$ 452. $^1$H NMR ($CD_3CN$, 298 K): $\delta_H$ 8.89 (2H, d, $J$ = 8.7, H(3)/H(12)), 8.26 (2H, s, H(9)/H(10)), 8.10 (2H, d, $J$ = 8.7, H(4)/H(11)), 5.36 (2H, d, $J$ = 24.0, H(1a)/H(14a) or (H(1b)/H(14b)), 4.98 (2H, d, $J$ = 24.8 Hz, H(1b)/H(14b) or H(1a)/H(14a)), 4.20–4.11 (2H, m, H(15a)/H(18a) or H(15b)/H(18b)), 3.79–3.73 (2H, m, H(15b)/H(18b) or H(15a)/H(18a)), 3.57–3.53 (4H, m, H(16)/H(17)). $^{13}$C NMR ($CD_3CN$, 298 K): $\delta_C$ 164.9, 147.5, 141.6, 131.3, 128.7, 125.5, 65.4, 50.5, 40.6. Electronic spectrum (MeCN): $\lambda$ = 281 ($\varepsilon$ = 34650), 356 (1880), 338 nm (2560 dm$^3$ mol$^{-1}$ cm$^{-1}$). Laminar crystals were also isolated after crystallisation corresponding to the formulation [Pd(**L**)][$BF_4$]$_2 \cdot \frac{1}{2}$MeCN.

**[Pt(L)][$BF_4$]$_2$.** A mixture of **L** (50 mg, 0.146 mmol) and $PtCl_2$ (40 mg, 0.146 mmol) in MeCN–water (40 cm$^3$, 1 : 1 v/v) was refluxed under $N_2$ for 6 h. Addition of a large excess of $NH_4BF_4$ to the resulting solution and concentration under reduced pressure afforded a yellow solid which was re-crystallised from MeCN–$Et_2O$ to give a yellow-brown microcrystalline powder (53 mg, 51% yield). FAB mass spectrum (3-NOBA matrix): $m/z$ 536; calc. for [$^{195}$Pt(**L**)]$^+$ 537. $^1$H NMR ($CD_3CN$, 298 K): $\delta_H$ 8.85 (2H, d, $J$ = 8.8), 8.15 (2H, s), 8.11 (2H, d, $J$ = 8.9), 5.39 (2H, d, $J$ = 18.8), 4.99 (2H, d, $J$ = 18.8 Hz), 4.06–4.04 (2H, m), 3.71–3.65 (2H, m), 3.60–3.54 (4H, m) [see [Pd(**L**)][$BF_4$]$_2$ for assignments]. $^{13}$C NMR ($CD_3CN$, 298 K): $\delta_C$ 163.9, 141.7, 131.2, 128.7, 124.9, 125.7, 66.4, 52.1, 41.9. Electronic spectrum (MeCN): $\lambda$ = 273 ($\varepsilon$ = 20250), 284 (21770), 309 (7640), 344 (1600), 361 nm (1100 dm$^3$ mol$^{-1}$ cm$^{-1}$).

**[Rh(L)$Cl_2$]$BF_4$.** A mixture of **L** (54 mg, 0.158 mmol) and $RhCl_3$ (33 mg, 0.158 mmol) in MeCN–water (40 cm$^3$, 1 : 1 v/v) was refluxed under $N_2$ for 5 h. Addition of a large excess of $NH_4BF_4$ to the resulting solution and partial removal of the

solvent under reduced pressure afforded a yellow solid (83 mg, yield 80%). Re-crystallisation by slow diffusion of $Et_2O$ vapour into an MeCN solution of the collected powder gave yellow platy crystals of $[Rh(\mathbf{L})Cl_2]BF_4$. FAB mass spectrum (3-NOBA matrix): *m*/*z* 515, 480 and 445; calc. for $[^{103}Rh(\mathbf{L})Cl_2]^+$, $[^{103}Rh(\mathbf{L})Cl]^+$ and $[^{103}Rh(\mathbf{L})]^+$ 516, 480 and 445 respectively. $^1$H NMR (dimethyl sulfoxide-$d_6$, 298 K): $\delta_H$ 9.18 (2H, d, $J$ = 8.4), 8.57 (2H, s), 8.49 (2H, d, $J$ = 8.4), 5.76 (2H, d, $J$ = 17.6), 5.53 (2H, d, $J$ = 18.0 Hz), 4.36–4.33 (2H, m, H(15a)/H(18a) or H(15b)/H(18b)), 4.09–3.99 (4H, m, H(16)/H(17)), 4.00–3.57 (2H, m, H(15b)/H(18b) or H(15a)/H(18a)) [see $[Pd(\mathbf{L})][BF_4]_2$ for the assignment of the other peaks in the aromatic region]. $^{13}$C NMR ($CD_3CN$, 298 K): $\delta_C$ 161.0, 140.1, 131.5, 128.6, 125.7, 66.1, 50.3, 36.6. Owing to the low solubility of the product in MeCN no electronic spectrum could be obtained.

**$[Ru(\mathbf{L})(PPh_3)][PF_6]_2\cdot\frac{1}{4}$MeCN.** A mixture of **L** (50 mg, 0.146 mmol) and $RuCl_2(PPh_3)_4$ (180 mg, 0.146 mmol) in MeOH (15 $cm^3$) was refluxed under $N_2$ for 2 h. Addition of a large excess of $NH_4PF_6$ afforded a yellow microcrystalline solid which was filtered off, washed with water and dried under reduced pressure (87 mg, yield 47%). Re-crystallisation by slow diffusion of $Et_2O$ vapour into a MeCN–MeOH solution of the product gave yellow platy crystals of $[Ru(\mathbf{L})(PPh_3)][PF_6]_2\cdot\frac{1}{4}$MeCN. FAB mass spectrum (3-NOBA matrix): *m*/*z* 851, 705 and 444; calc. for $[^{102}Ru(PPh_3)(\mathbf{L})PF_6]^+$, $[^{102}Ru(PPh_3)(\mathbf{L})]^+$ and $[^{102}Ru(\mathbf{L})]^+$ 850, 705 and 443 respectively. $^1$H NMR ($CD_3CN$, 298 K): $\delta_H$ 8.65 (2H, d, $J$ = 8.4), 8.33 (2H, s), 7.92 (2H, d, $J$ = 8.8), 4.51 (2H, d, $J$ = 19.2), 3.94 (2H, d, $J$ = 19.2 Hz), 3.30–3.10 (8H, m, H(16)/H(17) and H(15)/H(18)) [see $[Pd(\mathbf{L})][BF_4]_2$ for the assignment of the other peaks in the aromatic region]. $^{13}$C NMR ($CD_3CN$, 298 K): $\delta_C$ 163.6, 147.6, 137.3, 130.7, 128.5, 123.9, 76.6, 49.9, 40.4. Electronic spectrum (MeCN): $\lambda$ = 267 ($\varepsilon$ = 1270), 358 (199), 409 nm (191 $dm^3\ mol^{-1}\ cm^{-1}$).

**$[Ru(\mathbf{L}')Cl]Cl\cdot4H_2O$.** A suspension of **L′** (50 mg, 0.14 mmol) and $RuCl_2(PPh_3)_4$ (100 mg, 0.14 mmol) in ethanol (40 $cm^3$) was refluxed under nitrogen during two hours and the resulting red solution cooled to room temperature. A red microcrystalline solid appeared after slow evaporation of the solvent and this was filtered off, washed with *n*-hexane and re-crystallised from methanol to afford red crystals of $[Ru(\mathbf{L}')Cl]Cl\cdot4H_2O$ (56 mg, 76% yield) suitable for X-ray diffraction analysis. FAB mass spectrum (3-NOBA matrix): *m*/*z* 495, 460; calc. for $[^{102}Ru(\mathbf{L}')Cl]^+$ and $[^{102}Ru(\mathbf{L}')]^+$ 495 and 459 respectively. $^1$H NMR (dimethyl sulfoxide-$d_6$, 298 K): $\delta_H$ 8.77 (2H, d, $J$ = 8.4), 8.4 (2H, s), 8.3 (2H, d, $J$ = 8.8), 5.22 (2H, d, $J$ = 18.4), 5.02 (2H, d, $J$ = 19.2 Hz), 3.29–3.21 (2H, m, H(16a)/H(17a) or H(16b)/H(17b)), 3.17–3.10 (2H, m, H(16b)/H(17b) or H(16a)/H(17a)), 3.0–2.93 (2H, m, H(15a)/H(18a) or H(15b)/H(18b)), 2.91–2.87 (2H, m, H(15b)/H(18b) or H(15a)/H(18a)) [see $[Pd(\mathbf{L})][BF_4]_2$ for the assignment of the other peaks in the aromatic region]. $^{13}$C NMR (dimethyl sulfoxide-$d_6$, 298 K): $\delta_C$ 160.9, 146.5, 133.5, 128.8, 126.6, 122.3, 49.6, 37.1, 35.7. Electronic spectrum (MeCN): $\lambda$ = 420 ($\varepsilon$ = 3840), 489 nm (2990 $dm^3\ mol^{-1}\ cm^{-1}$).

## Crystallography

Crystal data and details of all six structure determinations appear in Table 3. Only special features of the analyses are noted here. Single crystal data collections for $\mathbf{L}\cdot\frac{1}{2}H_2O$, $[Ni(\mathbf{L})Cl]BF_4$, $[Pd(\mathbf{L})][BF_4]_2\cdot\frac{1}{2}$MeCN and $[Ru(\mathbf{L})(PPh_3)][PF_6]_2\cdot\frac{1}{4}$MeCN were performed on a Stoë Stadi-4 four-circle diffractometer using $\omega$–$\theta$ scans and crystals were cooled using an Oxford Cryosystem open flow cryostat.[40] For $[Ru(\mathbf{L}')Cl]Cl\cdot4H_2O$ and $[Pd(\mathbf{L})][BF_4]_2$ data were acquired at room temperature on a Rigaku AFC5S diffractometer using $\omega$–2$\theta$ scans and on a Enraf Nonius CAD4 diffractometer using $\omega$ scans, respectively. All datasets were corrected for Lorentz-polarisation effects and for absorption as specified in Table 3. The structures were solved by direct methods using SHELXS 97[41] and full-matrix

**Table 3** Crystallographic data

| | $\mathbf{L}\cdot\frac{1}{2}H_2O$ | $[Ni(\mathbf{L})Cl]BF_4$ | $[Pd(\mathbf{L})][BF_4]_2$ | $[Pd(\mathbf{L})][BF_4]_2\cdot\frac{1}{2}$MeCN | $[Ru(\mathbf{L})(PPh_3)][PF_6]_2\cdot\frac{1}{4}$MeCN | $[Ru(\mathbf{L}')Cl]Cl\cdot4H_2O$ |
|---|---|---|---|---|---|---|
| Formula | $C_{18}H_{19}N_2O_{1.5}S_2$ | $C_{18}H_{18}BClF_4N_2NiOS_2$ | $C_{18}H_{18}B_2F_8N_2OPdS_2$ | $C_{19}H_{19.5}B_2F_8N_{2.5}OPdS_2$ | $C_{36.5}H_{33.75}F_{12}N_{2.25}OP_3RuS_2$ | $C_{18}H_{26}Cl_2N_2O_4RuS_3$ |
| $M$ | 351.47 | 523.43 | 622.48 | 643.01 | 1006.01 | 602.56 |
| Crystal system | Triclinic | Monoclinic | Triclinic | Monoclinic | Monoclinic | Triclinic |
| Space group | $P\bar{1}$ (no. 2) | $P2_1/c$ (no. 14) | $P\bar{1}$ (no. 2) | $C2/m$ (no. 12) | $I2/a$ (no. 15) | $P\bar{1}$ (no. 2) |
| $a$/Å | 10.501(2) | 13.730(2) | 9.220(2) | 13.177(4) | 25.13(2) | 11.780(1) |
| $b$/Å | 13.314(3) | 13.853(3) | 11.025(2) | 11.520(4) | 12.55(2) | 14.619(1) |
| $c$/Å | 13.579(5) | 10.593(2) | 11.695(2) | 15.006(3) | 25.98(2) | 7.6281(8) |
| $\alpha$/° | 112.66(3) | | 96.68(2) | | | 104.260(9) |
| $\beta$/° | 95.78(4) | 101.97(2) | 98.27(2) | 95.83(5) | 99.15(5) | 95.42(1) |
| $\gamma$/° | 101.85(2) | | 112.04(2) | | | 67.081(7) |
| $V$/Å$^3$ | 1680.3(8) | 1971.0(6) | 1071.4(4) | 2266.0(11) | 8089(16) | 1172.7(2) |
| $Z$ | 4 | 4 | 2 | 4 | 8 | 2 |
| $T$/K | 150(2) | 150(2) | 293(2) | 210(2) | 150(2) | 294(2) |
| $\mu$(Mo-K$\alpha$)/mm$^{-1}$ | 0.326 | 1.383 | 1.146 | 1.088 | 0.699 | 1.191 |
| Reflections collected | 5962 | 3492 | 3745 | 2128 | 8760 | 4342 |
| Unique reflections, $R_{int}$ | 5962 | 3492 | 3745 | 2093, 0.128 | 7958, 0.044 | 4113, 0.013 |
| Reflections with $I \geq 2\sigma(I)$ | 5287 | 2774 | 3305 | 1818 | 5843 | 3386 |
| Absorption correction | None | Numerical | $\psi$ Scan | Numerical | $\psi$ Scan | $\psi$ Scan |
| $R1$ | 0.0497 | 0.0498 | 0.0457 | 0.0710 | 0.0585 | 0.0435 |
| $wR2$[all data] | 0.1380 | 0.1180 | 0.1219 | 0.1893 | 0.1561 | 0.1352 |

least-squares refinements on $F^2$ were performed using SHELXL 97.[42] For $[Pd(\mathbf{L})][BF_4]_2$ the structure was solved by a combination of Patterson and Fourier-difference synthesis using SHELXS 97.[41] All non-H atoms were refined anisotropically and H atoms were placed geometrically and thereafter allowed to ride on their parent atoms. In $\mathbf{L}\cdot\frac{1}{2}H_2O$ disorder was identified in the aliphatic portion of one of the two crystallographically independent macrocyclic units (B in Fig. 2) and modelled by using partial occupancy over two sites with a factor of 0.86 for the major component. In $[Pd(\mathbf{L})][BF_4]_2\cdot\frac{1}{2}$MeCN the O-donor lying on a crystallographic mirror plane was disordered, 0.70 of the occupation being by O(1) and 0.30 by O(1′). The MeCN solvent molecule was only partially occupied and also disordered across an inversion centre. Modelling involved the use of extensive positional and displacement parameter constraints and restraints for overlapping C and N atoms. The H atoms could not be included in the refinement model. One of the two $PF_6^-$ counter anions in $[Ru(\mathbf{L})(PPh_3)][PF_6]_2\cdot\frac{1}{4}$MeCN was found to be disordered. The disorder was modelled by a partial occupancy over two sites for each of the F atoms in the equatorial plane, converging with factors of 0.68 and 0.32. The two F atoms in the axial positions could be modelled as ordered. All the P–F bond distances were restrained to be the same during refinement, as were the F–P–F angles. Finally, in $[Ru(\mathbf{L}')Cl]Cl\cdot 4H_2O$ one of the water molecules was equally disordered over two sites. None of the H atoms in any of the four water molecules could reliably be positioned.

CCDC reference numbers 156508–156513.

See http://www.rsc.org/suppdata/dt/b1/b100493j/ for crystallographic data in CIF or other electronic format.

## Acknowledgements

We thank the "Comitato Nazionale per le Scienze Chimiche" of CNR of Rome and the EPRSC and University of Nottingham (UK) for financial support, Drs. Steve Davies and Johnathan McMaster for helpful discussions. We also acknowledge Professor Giuseppe Saba for hosting calculations on his workstation. J. C and V. M. acknowledge with thanks the financial assistance of Comision Interministerial de Ciencia y Tecnologia (C.I.C.Y.T.) of the Spanish Government provided by the project MAT97-0720. Support from the Academy of Finland is acknowledged by R. K.

## References

1 *Macrocyclic Compounds in Analytical Chemistry*, ed. Y. A. Zolotov, John Wiley & Sons, Inc., New York, 1997.
2 K. Kimura and T. Shono, in *Cation Binding by Macrocycles*, eds. Y. Inoue and G. W. Gokel, Marcel Dekker, New York, 1990.
3 J. S. Bradshaw and R. M. Izatt, *Acc. Chem. Res.*, 1997, **30**, 338.
4 P. Buhlmann, E. Pretsch and E. Bakker, *Chem. Rev.*, 1998, **98**, 1593.
5 A. T. Yordanov and D. M. Roundhill, *Coord. Chem. Rev.*, 1998, **170**, 93.
6 G. Khayatian and M. Shamsipur, *Sep. Purif. Technol.*, 1999, **16**, 235.
7 R. M. Izatt, K. Pawlak, J. S. Bradshaw and R. L. Bruening, *Chem. Rev.*, 1991, **91**, 1721.
8 A. J. Blake and M. Schröder, *Adv. Inorg. Chem.*, 1990, **35**, 1.
9 C. E. Housecroft, *Coord. Chem. Rev.*, 1992, **115**, 141.
10 J. Casabò, L. Mistres, F. Teixidor, L. Escriche and C. Pirez-Jiminez, *J. Chem. Soc.*, *Dalton Trans.*, 1991, 1969.
11 M. P. Almajano, L. Escriche, J. Casabò, R. Sillampää and R. Kivekas, *J. Chem. Soc.*, *Dalton Trans.*, 1992, 2889.
12 J. Casabò, F. Teixidor, L. Escriche, C. Viqas and C. Piréz-Jiménez, *Adv. Mater.*, 1995, **7**, 238.
13 A. J. Blake, F. Demartin, F. A. Devillanova, A. Garau, F. Isaia, V. Lippolis, M. Schröder and G. Verani, *J. Chem. Soc.*, *Dalton Trans.*, 1996, 3705.
14 F. Contu, F. Demartin, F. A. Devillanova, A. Garau, F. Isaia, V. Lippolis, A. Salis and G. Verani, *J. Chem. Soc.*, *Dalton Trans.*, 1997, 4401.
15 A. J. Blake, J. Casabò, F. A. Devillanova, L. Escriche, A. Garau, F. Isaia, V. Lippolis, R. Kivekas, V. Muns, M. Schröder, R. Sillampää and G. Verani, *J. Chem. Soc.*, *Dalton Trans.*, 1999, 1085.
16 A. J. Blake, F. A. Devillanova, A. Garau, F. Isaia, V. Lippolis, F. Silva and P. A. Vigato, in preparation.
17 J. Casabò, L. Escriche, S. Alegret, C. Jaime, C. Pèrez-Jimènez, L. Mestres, J. Rius, E. Molins, C. Miravitlles and F. Teixidor, *Inorg. Chem.*, 1991, **30**, 1893.
18 R. E. Wolf, J.-A. R. Hartman, J. E. M. Storey, B. M. Foxman and S. R. Cooper, *J. Am. Chem. Soc.*, 1987, **109**, 4328.
19 F. Arnaud-Neu, M.-J. Schwing-Well, R. Louis and R. Weiss, *Inorg. Chem.*, 1979, **18**, 2956.
20 M. Y. Darensbourg, I. Font, D. K. Mills, M. Pala and J. H. Reibenspies, *Inorg. Chem.*, 1992, **31**, 4965.
21 J. E. Huheey, E. A. Keiter and R. L. Keiter, *Inorganic Chemistry; Principles of Structures and Reactivity*, 4th edn., Harper Collins, New York, 1993, Table 8.1, p. 292.
22 C. R. Lucas, W. Liang, D. O. Miller and J. N. Bridson, *Inorg. Chem.*, 1997, **36**, 4508.
23 R. Louis, D. Pelissard and R. Weiss, *Acta Crystallogr.*, *Sect. B*, 1974, **30**, 1889.
24 A. R. Rossi and R. Hoffmann, *Inorg. Chem.*, 1975, **14**, 365.
25 A. J. Blake, G. Reid and M. Schröder, *Polyhedron*, 1992, **19**, 2501.
26 A. J. Blake, G. Reid and M. Schröder, *J. Chem. Soc.*, *Dalton Trans.*, 1989, 1675.
27 M. E Sosa and M. L Tobe, *J. Chem. Soc.*, *Dalton Trans.*, 1986, 427.
28 P. F. Kelly, W. Levason, G. Reid and D. J. Williams, *J. Chem. Soc.*, *Chem. Commun.*, 1993, 1716.
29 M. Schröder, *Pure Appl. Chem.*, 1988, **4**, 517.
30 B. Chack, A. McAuley and T. Whitcombe, *Can. J. Chem.*, 1994, **72**, 1525.
31 A. J. Blake, G. Reid and M. Schröder, *J. Chem. Soc.*, *Dalton Trans.*, 1990, 3363.
32 A. J. Blake, Y. V. Roberts and M. Schröder, *J. Chem. Soc.*, *Dalton Trans.*, 1996, 1885.
33 D. E. Morris, K. W. Hanck and M. K. DeArmond, *J. Am. Chem. Soc.*, 1983, **105**, 3032.
34 V. W.-W. Yam, V. W.-M. Lee, F. Ke and K.-W. M. Siu, *Inorg. Chem.*, 1997, **36**, 2124.
35 Spartan Version 5.0, Wavefunction Inc., 18401 Von Karman Ave., Ste. 370, Irvine, CA 92612, USA.
36 T. A. Halgren, *J. Comput. Chem.*, 1996, **17**, 490.
37 C. J. Chandler, L. W. Deady and J. A. Reiss, *J. Heterocycl. Chem.*, 1981, **18**, 599.
38 B. DeGroot and S. J. Loeb, *Inorg. Chem.*, 1989, **28**, 3573.
39 P. S. Hallman, T. A. Stephenson and G. Wilkinson, *Inorg. Synth.*, 1970, **12**, 237.
40 J. Cosier and A. M. Glazer, *J. Appl. Crystallogr.*, 1986, **19**, 105.
41 G. M. Sheldrick, SHELXS 97, *Acta Crystallogr.*, *Sect A*, 1990, **46**, 467.
42 G. M. Sheldrick, SHELXL 97, Universität Göttingen, 1997.